liquids

MDPI

Article

A Coherent Electrodynamics Theory of Liquid Water

Antonella De Ninno [1,*] and Luca Gamberale [2,3,4]

[1] ENEA Frascati Research Center, Via Enrico Fermi 45, 00044 Frascati, Italy
[2] Quantumatter Inc., 277 West End Ave. #7D, New York, NY 10023, USA; luca.gamberale@unimib.it
[3] Leda Srl, Corso Monforte 19, 20122 Milano, Italy
[4] Physics Department, University of Milano-Bicocca, Piazza della Scienza 3, 20126 Milano, Italy
* Correspondence: antonella.deninno@enea.it

Abstract

This study presents a quantum electrodynamics (QED) framework that explains the anomalous behavior of liquid water. The theory posits that water consists of two coexisting phases: a coherent phase, in which molecules form phase-locked coherence domains (CDs), and an incoherent phase that behaves like a dense van der Waals fluid. By solving polynomial-type equations, we derive key thermodynamic properties, including the minima in the isobaric heat capacity per particle (IHCP) and the isothermal compressibility, as well as the divergent behavior observed near 228 K. The theory also accounts for water's high static dielectric constant. These results emerge from first-principles QED, integrating quantum coherence with macroscopic thermodynamics. The framework offers a unified explanation for water's anomalies and has implications for biological systems, materials science, and fundamental physics. Future work will extend the theory to include phase transitions, solute interactions, and the freezing process.

Keywords: liquid water thermodynamics; coherent domains (CDs); quantum electrodynamics (QED); two-phase model of water; energy gap in coherent water; isobaric heat capacity anomalies; isothermal compressibility of water; static dielectric constant of liquid water; spontaneous symmetry breaking in water; coherent—incoherent phase equilibrium

Academic Editors: Darin J. Ulness and Enrico Bodo

Received: 25 July 2025
Revised: 9 October 2025
Accepted: 15 October 2025
Published: 5 November 2025

Citation: De Ninno, A.; Gamberale, L. A Coherent Electrodynamics Theory of Liquid Water. *Liquids* **2025**, *1*, 30. https://doi.org/10.3390/liquids5040030

1. Introduction

The enigmatic behavior of liquid water, illustrated by phenomena such as its maximum density, maximum isothermal compressibility, very high thermal capacity, and ultra-high dielectric constant, has fueled scientific inquiry for more than a century. These are just a few of many thermodynamic properties in which water deviates significantly from the behavior of simple liquids. In 1892, Roengten first speculated that water comprises interpenetrating "ice-like" and "fluid" structures, a classical mixture model that laid the groundwork for later two-phase theories [1].

Parallel developments in classical physics gained momentum with the evidence of metastable coexistence of low-density liquids (LDL) and high-density liquids (HDL) in supercooled water [2]. This was corroborated by Mishima et al. through pressure-induced amorphous ice transitions [3], while Wernet et al. used X-ray spectroscopy to identify structural motifs similar to LDL and HDL in ambient water [4].

In fact, different experimental techniques such as small-angle X-ray scattering (SAXS) and Kerr effect in liquid water show the existence of two different fluids normally interpreted as hydrogen-bond networks and individual modes governed by collisional

processes [5,6]. Modern studies highlight both numerically and experimentally that thermodynamic anomalies are signatures of the existence of two separate intertwined phases [7,8].

The two-structure model supported by MD simulations stems from numerical analyses with the ST2 water-like empirical potential [9]. In the past three decades, computational modelling has been strongly improved by the data-driven many-body potentials. Among these, MB-pol [10] has provided a realistic representation of water across all phases and leads to a good interpretation of the density anomaly [11]. However, the great complexity of the calculations requires sophisticated mathematical tools and deep neural network models (e.g., DNN@MB-pol) derived from extensive sets of configurations. While the thermodynamic quantities obtained by such methods can reproduce the related phenomena, it is often difficult to discuss the underlying thermodynamic mechanisms in direct relation to the specific shapes of the intermolecular interactions. Such an approach describes some of the so-called water anomalies but may fail to provide a comprehensive physical description of the water system and to predict its behavior outside the range of conditions covered by the simulation.

Another approach considers that the intermolecular interactions in water are constantly changing depending on the state of thermal equilibrium [12]. However, as the author notes: "At present, it is impossible to derive the functional shapes of intermolecular interactions in water from basic equations such as the Schrödinger equation. The validity of the shapes must be judged by whether the assumed functional shapes can reproduce the measured values of some thermodynamic quantities of water". A potential risk is that the best fit of experimental data using different parameters can lead to different functional shapes.

A radical departure emerged in the 1980s with the quantum electrodynamic (QED) framework by Del Giudice and Preparata, who proposed that water sustains macroscopic coherence through photon-exchange interactions, forming ordered "coherent domains" (CDs) alongside disordered bulk regions [13,14]. In 2012 Del Giudice et al. refined the calculations showing that water molecules can undergo phase transitions to a coherent condensed phase, oscillating in unison with a self-trapped electromagnetic field. Such configurations imply the existence of quasi-free electrons capable of explaining a large number of biological phenomena [15].

In this paper, we follow the lines initially delineated by Preparata and Del Giudice [14,16] by developing the thermodynamics of the coherent and incoherent phases making the assumption that the incoherent phase behaves essentially as a polar van der Waals (vdW) fluid. Part I will provide a detailed exposition of the theory, while Part II will explore the thermodynamic properties of liquid water as derived from it. This approach will lead us to explain the origin of thermal anomalies such as density and thermal expansion (Section 3.3), isobaric heat capacity per particle(IHCP) (Section 3.4), isothermal compressibility (Section 3.5). We will use natural units where $\hbar = k_B = c = 1$.

2. Part I

2.1. Physics of the Two Fluids

It is universally accepted that the most accurate description of phenomena in condensed matter lies in the realm of quantum electrodynamics (QED). Water is no exception. However, due to the enormous difficulty of the mathematical task, the solution of the equations of water physics is often approximated using semiclassical or classical models, in which the interactions between molecules are described via phenomenological potentials. The solution of the resulting classical many-body equations of motion is left to the numerical calculations of powerful computers. The thermodynamic variables are calculated by averaging the dynamic configurations over a large number of particles.

This approach, although very popular, has significant limitations due to the limited power of the available computers such as the low number of water molecules that can be simulated and the very short evolution times of the dynamic equations that can be reached. Perhaps more importantly, the potentials that are used to describe the interactions among molecules arise from phenomenological arguments rather than from first principles.

Here we approach the two-fluid picture of liquid water having its origins into the existence of a spontaneous symmetry breaking mechanism of the electromagnetic field in interaction with the water molecules. This approach was first proposed in the late 1980s by a group of Italian theoretical physicists who used high-energy physics methods to the condensed matter. The results that emerged were surprising in many ways but did not meet with the favor of the community of physicists historically engaged in the study of water, both because of the natural distrust towards colleagues from another sector and because of the methodology based on analytical calculation rather than on molecular dynamics simulations that were increasingly gaining ground in those years.

Recent advances in quantum electrodynamics (QED) have revealed that coherent domains (CDs) emerge through spontaneous symmetry breaking of the electromagnetic field in interaction with water molecules. This results in a macroscopic quantum ground state distinct from individual molecular states, as demonstrated in [15–18]. Experimental validation comes from [19], showing that vibrational spectra reveal that liquid water can be described as a mixture of high-density and low-density fractions. In Ref. [20], it is argued that the existence of a low-density, low-entropy phase in bulk water organized in tiny patches is necessary to explain the experimental observations.

After many decades, the two-fluid structure of water, initially strongly contested, is now accepted by most scientists even if the justification given is largely phenomenological. By recovering the QED approach, we obtain an analytical and accurate description of the structural, dynamic and thermodynamic properties of water that allows not only to explain the still unexplained experimental results but also to face the deep implications for biological systems, material science, and fundamental physics.

In the following are the main outcomes of the QED theory of water.

(1) Liquid water is composed by two different mixed fractions over the whole range of existence of the liquid: a *coherent* phase where molecules are phase-locked over an extended space-time region and a *incoherent* (or *normal*) phase made up of individual molecules forming a dense incoherent fluid. The two phases are interspersed and cannot be separated as in the case of the two-fluids model of superfluid ^{4}He. As a general rule, the incoherent phase predominates at high temperatures and gradually decreases in favor of the coherent phase with decreasing temperature in a way that will be described in the following paragraphs.

(2) The coherent phase is made up by an ensemble of *Coherence Domains* (CDs) that can be assumed as spheres whose radius depends on the temperature. The centers of the CDs are arranged in a regular configuration in order to minimize the energy of the system. When the temperature decreases, the CDs tend to increase their size until they merge into a single macroscopic domain for sufficiently low temperature. This may account for increased viscosity when temperature is decreased and may account for the glassy nature of supercooled water [21].

(3) The molecules belonging to the coherent phase are energetically separated from the non-coherent phase by an *energy gap*, protecting them from the thermal fluctuations. The reason of the existence of an energy gap is due to a collective ground state different from the *perturbative* ground state of the isolated molecules [16].

(4) The single CD at zero temperature is characterized by a collective interaction among the water molecules through a macroscopic coherent electromagnetic field. These molecules are kept in phase by the electromagnetic field whose profile is given by [16]

$$g_1(r) = \begin{cases} \frac{\sin(\pi x)}{\pi x} & \text{if } x < 3/4 \\ \frac{e^{\pi(\frac{3}{4}-x)}}{\pi\sqrt{2x}} & \text{if } x > 3/4 \end{cases} \quad (1)$$

where $x = r/r_{CD}$, r is the radial distance from the center of the CD and r_{CD} ∼38 nm is the CD radius. The profile of the energy gap per particle for a single CD is given by $\delta_c(r) = \delta_0 g_1^2(r)$, since the energy per particle is proportional to the square of the amplitude of the coherent electromagnetic field.

(5) The CDs are arranged in a HPC configuration in order to minimize the total energy. As the temperature increases, the molecules belonging to the coherent state migrate towards the incoherent state, thus reducing the coherent fraction. A fluid of incoherent molecules is then formed which fills the interstices between the CDs and the size of the CDs gets reduced. It is worth noting that the arrangement of the CDs does not form a rigid crystal, as each CD can slide over the adjacent ones, separated by the incoherent fluid.

In Figures 1 and 2 are shown the spatial arrangement of the CDs and the contouring map of $\Gamma(\vec{x})$

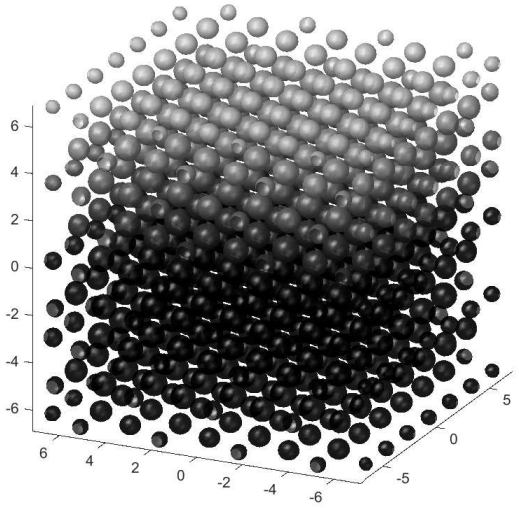

Figure 1. HPC arrangement of the CDs. Units are CD diameters.

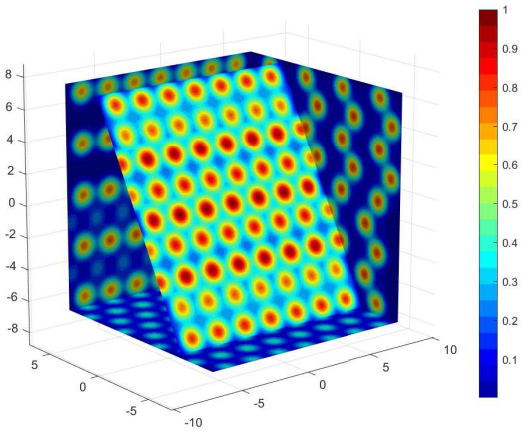

Figure 2. Color contouring map of the profile function $\Gamma^2(\vec{x})$. Units are CD diameters.

(6) At a fixed temperature T and pressure P the total number of molecules N can be written as $N = N_c(T,P) + N_n(T,P) + N_v(T,P)$, being N_c the number of molecules in the coherent phase, N_n the number of molecules in the incoherent phase and N_v the number of molecules in the vapor phase.

(7) The molecules belonging to the coherent phase are in an excited electronic state given by the superposition of the ground state $|0\rangle$ and the excited state $|5d\rangle$ corresponding to an energy of 12.06 eV according to the formula

$$|\text{coherent}\rangle = \cos\alpha|0\rangle + \sin\alpha|5d\rangle \quad (2)$$

with $\cos^2\alpha = 0.873$ [16], whose energy gap is $\delta_{0c} \simeq = -0.3$ eV per molecule. Since the excited state $|5d\rangle$ is spatially quite more extended than the ground state $|0\rangle$, the intermolecular distance is larger than would be predicted from the standard molecular size. Furthermore, the new electronic configuration accounts for the tetrahedral coordination of the water molecules in the coherent phase. In Ref. [22] this problem has been thoroughly discussed. This fact implies that the water molecules in the coherent phase are arranged in an ice-like spatial configuration.

(8) It is worth noting that the coherence involves the electronic levels $|0\rangle$ and the $|5d\rangle$ only, so that the nuclei of the molecules are still able to perform vibrations but not rotations limited to small angles around the equilibrium directions defined by the H-bonds that, in this context, are determined by the modified electronic distribution of the coherent water molecules [22]. The kinetic contribution to the partition function of the coherent phase is therefore purely vibrational.

(9) The incoherent phase is treated as a polar fluid, where interactions are governed by a combination of the Lennard-Jones potential and dipole-dipole forces. It remains in thermodynamic equilibrium with the coherent phase, with which it continuously exchanges particles. A rigorous approach to describing the many-body interactions within the incoherent phase would involve applying the Bogoliubov diagonalization procedure, leading to a gas of quasi-particles and a phonon/roton-like interpretation. This approach would provide a detailed understanding of the thermodynamic properties of the incoherent phase, as well as the propagation of sound in liquid water. However, in this study, we approximate the incoherent phase as a vdW liquid, whose thermodynamic properties are well established. Although this approximation does not fully capture certain characteristics of liquid water, particularly the pressure-temperature coexistence curve, our primary goal is to demonstrate the qualitative explanatory power of our theoretical framework.

(10) Solidification of liquid water (freezing) will not be taken into account in the present paper since it is related to the onset of a different type of electromagnetic symmetry breaking, leading to an energy gap of a different nature. The formation of ice will be the subject of a future work.

2.2. Definition of the Coherent Spatial Profile

The spatial modulation of the amplitude of both the matter field and the electromagnetic field within a single coherence domain is approximately described by the radial profile of the spherical Bessel function of the first kind, j_0. As shown in Reference [16] and mentioned in Section 2.1, the profile of a single coherence domain is given by Equation (1) that decays exponentially in the peripheral regions of the domain.

The presence of many packed domains causes the isolated domain's spherical symmetry to be lost. Therefore, we use the volumetric fraction ϕ_{vol} rather than the reduced radius to characterize the coherent phase:

$$\phi_{vol} = \frac{v_c}{v_{total}} \tag{3}$$

where v_c is the volume occupied by the coherent phase and v_{total} is the total volume occupied by the liquid, where we make the identification $\phi_{vol} \equiv x^3$.

By defining $\Gamma(\phi_{vol}) = g_1(\phi_{vol}^{1/3} r_{CD})$, the variation of the coherent gap as a function of the fractional volume is given by the square of the Γ function multiplied by the value of the energy gap at the center of the coherence domain, according to

$$\delta_c(\phi_{vol}) = \delta_{0c}\Gamma^2(\phi_{vol}). \tag{4}$$

Figure 3 illustrates the profile of the coherent electromagnetic field as a function of the coherent fractional volume ϕ_{vol} for an isolated single domain.

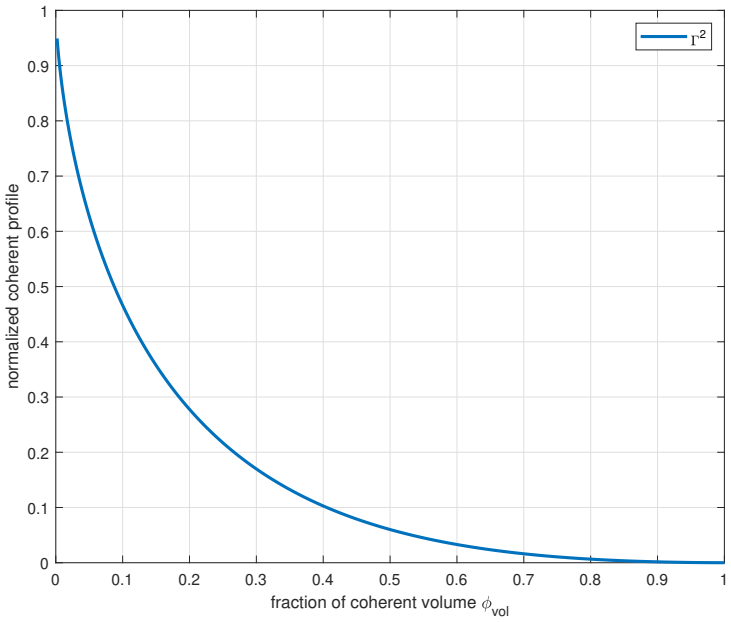

Figure 3. Normalized profile of the energy gap $\Gamma^2(\phi_{vol})$ as a function of the fractional coherent volume $\phi_{vol} = \frac{V_c}{V}$.

2.3. Free Energy of the Coherent Fluid

We now need to determine the thermodynamic potentials of the coherent and incoherent phases in order to obtain the relation between the thermodynamic variables P and T and the coherent phase.

The free energy per particle of the coherent phase can be expressed as:

$$f_c(\hat{\rho}_c, T, \phi_{vol}) = f_{c,\text{gap}}(\hat{\rho}_c, \phi_{vol}) + f_{c,\text{LJ}}(\hat{\rho}_c) + f_{c,\text{dd}} + f_{c,\text{vib}}(T), \tag{5}$$

where $\hat{\rho}_c = \frac{\rho_c}{\rho_0}$. The reference density ρ_0 corresponds to the density at which the Lennard-Jones potential reaches its minimum energy in the coherent phase and is treated as a free parameter in the following.

The coherent state, as a singular collective quantum state, is inherently defined at absolute zero temperature. This arises from the fundamental observation that, since the quantum phases of the electronic wavefunctions of individual molecules are locked to a common value, they cannot exhibit an arbitrary phase factor of the form $e^{i\vec{k}_n \cdot \vec{x}}$, which is characteristic of an ensemble of incoherent particles following a Boltzmann statistical distribution. As a result, the positional energy of the water molecules is independent of temperature.

This argument does not extend to the vibrational degrees of freedom of the water molecules, which exhibit normal thermodynamic behavior, as described below.

To characterize the short-range electrostatic interaction within the coherent phase, we utilize a Lennard-Jones potential. At absolute zero temperature, the single-particle free energy associated with this potential depends only on the density and is given by

$$f_{c,\mathrm{LJ}} = -\delta_{c\mathrm{LJ}}\hat{\rho}_c^2\left(2-\hat{\rho}_c^2\right), \tag{6}$$

where $\delta_{c\mathrm{LJ}}$ is taken as a free parameter (see Section 3.2). Note that ρ_0 and $\delta_{c\mathrm{LJ}}$ differ from those in the incoherent phase because the molecules in the coherent phase occupy an excited electronic state. As a result, they are larger than their incoherent counterparts, which in turn alters both the depth and equilibrium position of the Lennard-Jones potential (Figure 4). The values of ρ_0 and $\delta_{c\mathrm{LJ}}$ have been determined through numerical fitting of experimental data.

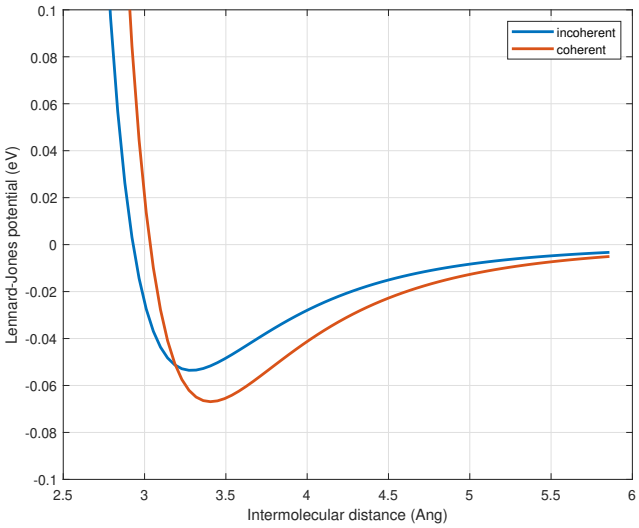

Figure 4. Comparison of the Lennard–Jones potential for the coherent and incoherent phases.

The free energy contribution due to the energy gap is given by:

$$f_{c,\mathrm{gap}} = -\delta_{0c}\Gamma^2(\phi_{vol})\hat{\rho}_c^b, \tag{7}$$

where $b = 0.84$ has been determined by a fit of the calculated energy gap as a function of density by solving numerically the equations in Refs. [16,18].

Due to the strong electrostatic forces generated by the coherent electronic configuration, the rotational motion of the molecules is almost entirely suppressed, reducing them to minor librations around their equilibrium positions.

Although the dipole-dipole positional energy could, in principle, be calculated numerically, in this analysis, we approximate it with a constant value, treated as a free parameter:

$$f_{c,\mathrm{dd}} = -\delta_{c,\mathrm{dd}}. \tag{8}$$

The vibrational dynamics of coherent water molecules, represented by $f_{c,\mathrm{vib}}$, is associated with the vibrations of the oxygen and hydrogen nuclei around their equilibrium positions and is restricted by the electrostatic cage imposed by the coherent electronic state. Each water molecule has 6 degrees of freedom, namely the librational motions around the three spatial axes, the two vibrational modes, asymmetric and symmetric stretching and the bending.

We will approximate their dynamics to the dynamics of one-dimensional harmonic oscillators so that their free energy can be written as:

$$f_{c,\mathrm{vib}} = T\sum_{\omega_i} g(\omega_i)\log\left[2\sinh\left(\frac{\omega_i}{2T}\right)\right], \tag{9}$$

where $g(\omega_i)$ represents the density of states that are normalized so as to fulfill the normalization condition:

$$\sum_{\omega_i} g(\omega_i) = \text{number of degrees of freedom} = 6. \tag{10}$$

The total number of degrees of freedom is six, consisting of three degrees of freedom associated with the librational motions around the three spatial axes, along with the two vibrational modes, asymmetric and symmetric stretching and bending.

The contributions from the asymmetric stretching, symmetric stretching, and bending modes, for which $\omega_i \gg T$, are essentially independent of temperature. As a result, Equation (9) can be approximated by:

$$f_{c,\mathrm{vib}} = T\sum_{\substack{i\\ \text{librational}}} g(\omega_i)\log\left[2\sinh\left(\frac{\omega_i}{2T}\right)\right] + \frac{1}{2}\sum_{\substack{i\\ \text{stretching}\\ \text{bending}}} g(\omega_i)\,\omega_i. \tag{11}$$

The free energy contribution from the higher-frequency modes thus becomes a temperature-independent constant, which can be incorporated into the additive fitting parameter $\delta_{c,\mathrm{dd}}$.

Although the total number of vibrational modes per molecule must be six, the actual distribution of the vibrational density of states $g(\omega_i)$ in liquid water is not known with certainty. Only low-energy modes (with $\omega \lesssim 100$ meV) contribute significantly to the thermodynamics at room temperature. This is because the Boltzmann factor $\exp(-\omega/T)$ strongly suppresses the contribution of modes with energy $\omega \gg T \approx 26$ meV—the characteristic thermal energy at 300 K—to the free energy. The assumed form of $g(\omega_i)$ used in this work is reported in Table 1, where we have approximated the spectral density of states as the sum of two delta functions, weighted with $g(\omega_i)$. These values play a key role in the determination of the isobaric heat capacity (see Section 3.4).

Table 1. Principal vibrational modes of the coherent fraction with corresponding spectral weights and energies.

Wavenumber (cm^{-1})	Spectral Weight $g(\omega)$	Energy (meV)
52	0.61	6.5
161	4.39	20

Finally, the relationship between pressure and density is given by:

$$\hat{P} = \hat{\rho}_c^2 \frac{\partial f_{c,\mathrm{tot}}}{\partial \hat{\rho}_c}, \tag{12}$$

where $\hat{P} = \frac{P}{\rho_0}$. Note that $\hat{P}$ is not uniform inside the coherent phase since the energy gap depends on the volumetric fraction ϕ_{vol}. Therefore, we need to compute pressure and density of the coherent phase as a function of ϕ_{vol}. We perform such a calculation in Section 2.5.

2.4. Free Energy of the Incoherent Fluid

An accurate description of the dynamics of the incoherent fraction would, in principle, require a Bogoliubov diagonalization of the matter field fluctuations around the coherent background configurations. In the present work, however, we adopt a simplified approach by modeling the incoherent phase as a van der Waals fluid. This approximation is quite crude in certain respects—most notably in its description of the pressure–temperature liquid–vapor coexistence curve—but it enables an algebraic formulation of the thermodynamic equations for the key parameters considered here. A more refined description will be addressed in a future treatment.

For the incoherent phase at equilibrium with the vapor, the free energy per particle is given by

$$f_n(P,T) = f_{n,\mathrm{vdW}}(P,T) + f_{n,\mathrm{dd}}(P,T) + f_{n,\mathrm{vib}}(T), \tag{13}$$

where

$$f_{n,\mathrm{vdW}}(P,T) = -T\left\{1 + \log\left[\left(\frac{mT}{2\pi}\right)^{\frac{3}{2}} \frac{1-b\rho_n(P,T)}{\rho_n(P,T)}\right]\right\} - a\rho_n(P,T) \tag{14}$$

is the van der Waals contribution to the free energy [23], with a and b being the standard van der Waals parameters. These are related to the critical temperature T_{crit} and critical pressure P_{crit} by the expressions

$$a = \frac{27T_{\mathrm{crit}}^2}{64P_{\mathrm{crit}}}, \tag{15a}$$

$$b = \frac{T_{\mathrm{crit}}}{8P_{\mathrm{crit}}}. \tag{15b}$$

The term $f_{n,dd}(P,T)$ represents the contribution due to dipole-dipole interactions. Liquid water is highly polar, being the dipole moment of vapor water molecule $\mu_{dd} = 1.85$ D [24], which is equivalent to $5.88 \cdot 10^{-5}$ eV^{-1}, and the strength of the interaction is controlled by the Debye-Langevin parameter $\alpha = \frac{\mu_{dd}^2 \rho_n}{3T}$ which in the whole thermal range of existence of the liquid is larger than 1, implying that the average energy of adjacent dipoles $\frac{\mu_{dd}^2 \rho_n}{3}$ is always larger than the average kinetic energy of the molecules $\frac{3}{2}T$. This observation suggests that the behavior of dipoles is inclined towards organizing themselves into quasi-crystalline formations, which results in the disruption of rotational symmetry. A basic computation of free energy by averaging over the orientations of dipoles does not furnish an accurate estimate of the free energy in this case. To achieve a more dependable assessment of this quantity, one might consider employing a numerical approach. This can be effectively achieved using computational techniques in molecular dynamics, which provide more precise insights into the system's free energy profile.

The generalized assertion that can be made is that, due to lack of the rotational symmetry, the free energy is linearly proportional to α rather than being proportional to α^2, which is the case in the regime where α is small. Consequently, we assume that the dipole-dipole free energy is proportional to the reduced density $\hat{\rho}_n = \frac{\rho_n}{\rho_{\mathrm{crit}}}$:

$$f_{n,dd}(P,T) = -\delta_{n,dd}\hat{\rho}_n. \tag{16}$$

However, this term should not be included in the free energy calculation to avoid double-counting its effects. The impact of this interaction is already reflected in the experimental values of the critical temperature T_{crit} and critical pressure P_{crit}. The key point is that including this term does not change the form of the free energy but only adjusts the value of the van der Waals coefficient a by $\delta_{dd}\rho_{\mathrm{crit}}$, which is already accounted for in the experimental data for P_{crit} and T_{crit}. Therefore, we set $\delta_{n,dd} = 0$ eV.

Finally, the term $f_{\text{vib}}(T)$ accounts for the residual dynamics of hindered rotations—molecular librations around equilibrium orientations—as well as for the vibrations of the hydrogen atoms, similarly to what was considered for the coherent phase.

As in the coherent case, we assume a total of six vibrational degrees of freedom: three associated with bending, asymmetric stretching, and symmetric stretching, and three corresponding to librational modes. However, as in the coherent phase, only the librational (low-energy) modes contribute significantly to the thermodynamics, since the higher-frequency modes remain essentially unexcited in the temperature range relevant for liquid water.

Although some difference in the vibrational density of states between the coherent and incoherent phases is expected especially in the stretching modes [17], in the present work we approximate the function $g(\omega_i)$ to be the same in both cases.

The vibrational free energy can therefore be written as

$$f_{n,\text{vib}} = f_{c,\text{vib}} + C, \tag{17}$$

where C is an unimportant constant that will be absorbed in the parameter $\delta_{\text{c,dd}}$.

In order to completely define Equation (14) we must express the density ρ_n in terms of P and T. This is accomplished through the equation of state of the vdW fluid

$$\hat{P}_n = \frac{8\hat{\rho}_n \hat{T}}{3 - \hat{\rho}_n} - 3\hat{\rho}_n^2 \tag{18}$$

where $\hat{P}_n = \frac{P_n}{P_{crit}}$ and $\hat{T} = \frac{T}{T_{crit}}$ are the reduced pressure and temperature of the vdW fluid. The density ρ_n can then be computed by numerically solving Equation (18).

2.5. Solution of the Equilibrium Equations and Calculation of the Coherent Fraction

The analysis of liquid water reveals a two-phase composition: an incoherent phase behaving as a polar vdW fluid, and a coherent phase consisting of coherence domains (CDs) of polar molecules at essentially zero translational temperature (though vibrational components remain incoherent). These phases coexist with the vapor phase along the liquid-vapor coexistence curve in the $P - T$ plane. The thermodynamics of this system involves determining the densities of all three phases and their equilibrium pressure.

While the vapor and incoherent phase pressures and densities are known from vdW solutions, the coherent domain's internal density and pressure require careful analysis due to spatial potential gradients.

For convenience we will isolate the positional component of the coherent free energy by defining the component independent of temperature f_{0K} as:

$$f_{0K} = f_c - f_{c,vib}. \tag{19}$$

At thermodynamic equilibrium, the chemical potentials of the coherent and incoherent phases must be equal at the CD boundary. The coherent chemical potential is given by:

$$\mu_c = f_{0K} + \frac{\tilde{P}_c}{\hat{\rho}_c} \tag{20}$$

where the tilde superscript means division by the reference density ρ_0, $\tilde{P}_c = \frac{P_c}{\rho_0}$ and is given by:

$$\tilde{P}_c = \hat{\rho}_c^2 \frac{\partial f_{0K}}{\partial \hat{\rho}_c}. \tag{21}$$

The solution requires solving the coupled equations for pressure equality and chemical potential equality at the CD boundary, which read

$$\mu_c(\hat{\rho}_c, \phi_{vol}) = \mu_0(T) \tag{22a}$$

$$\tilde{P}_c(\hat{\rho}_c, \phi_{vol}) = \tilde{P}_n(T) \tag{22b}$$

where $\mu_0(T) = f_n(T) + \frac{P_n}{\rho_n} - f_{c,vib}(T)$ and $\tilde{P}_n = \frac{P_n}{\rho_0}$.

Equations (22) determine both the coherent fraction ϕ_{vol} and the density profile within the CDs as a function of temperature along the liquid-vapor coexistence curve.

To solve for the equilibrium conditions, we can isolate $\Gamma^2(\phi_{vol})$ from both the chemical potential and pressure Equations (20) and (21). Equation (22a) can be reformulated as

$$\Gamma^2_{\mu}(\phi_{vol}) = \frac{\mu_0(T) - \delta_{cLJ}(\hat{\rho}_c^4 + 4\hat{\rho}_c^3 - 2\hat{\rho}_c^2 - 4\hat{\rho}_c)}{\delta_{0c}\hat{\rho}_c^b(1+b)}. \tag{23}$$

Similarly, from the pressure Equality (22b) at the boundary:

$$\Gamma^2_{P}(\phi_{vol}) = \frac{\tilde{P}_n - \delta_{cLJ}(4\hat{\rho}_c^4 - 4\hat{\rho}_c^2)}{\delta_{0c}b\hat{\rho}_c^{b+1}}. \tag{24}$$

The physical solution must satisfy both equations simultaneously, which means finding values of $\hat{\rho}_c$ where $\Gamma^2_{\mu}(\phi_{vol}) = \Gamma^2_{P}(\phi_{vol})$. This can be visualized by plotting both expressions as functions of $\hat{\rho}_c$ for different temperatures as shown in Figure 5.

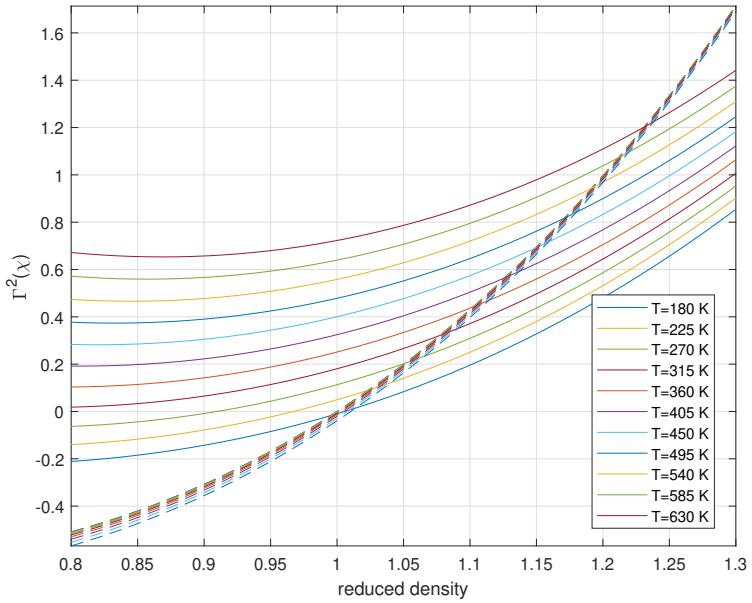

Figure 5. Solutions for $\Gamma^2(\phi_{vol})$ from chemical potential (solid lines) and pressure (dashed lines) equations at different temperatures. The intersections determine the physically meaningful solutions for the density at the CD boundary for $\Gamma^2(\phi_{vol})$ in the existence interval [0 1] only.

The intersection points provide both the equilibrium density at the CD boundary ($\hat{\rho}_c$, from the x-coordinate) and the corresponding value of $\Gamma^2(\phi_{vol})$ (from the y-coordinate) at each temperature. The value of $\Gamma^2(\phi_{vol})$ must be between 0 and 1 for physical solutions. When $\Gamma^2(\phi_{vol}) > 1$, the coherent fraction is 0, and when $\Gamma^2(\phi_{vol}) < 0$, the coherent fraction is 1.

The numerical solutions of Equation (22) are shown in Figure 6 for $\phi_{vol}(T)$ and in Figure 7 for the density (blue curve). Figure 8 shows the profile of reduced coherent density and pressure inside the coherent phase as a function of the inner reduced volume.

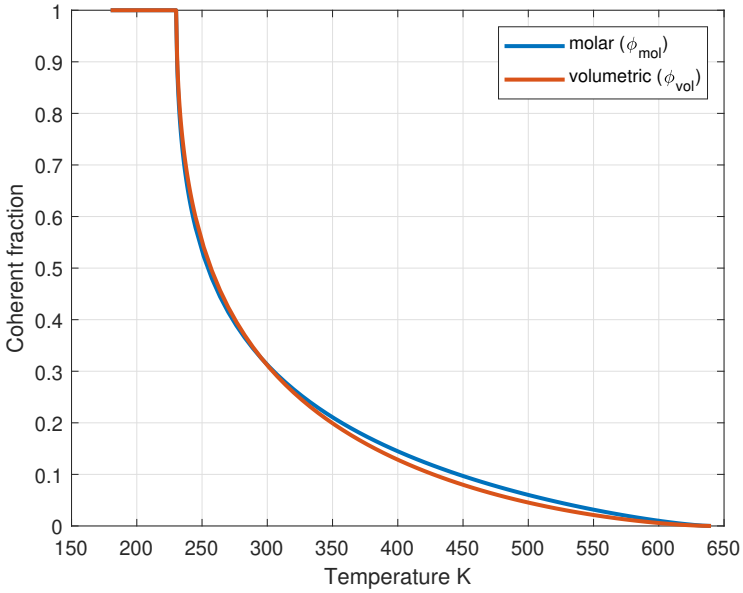

Figure 6. Temperature dependence of both molar and volumetric ($\phi_{vol}(T)$) coherent fractions, showing the transition from fully coherent to fully incoherent behavior.

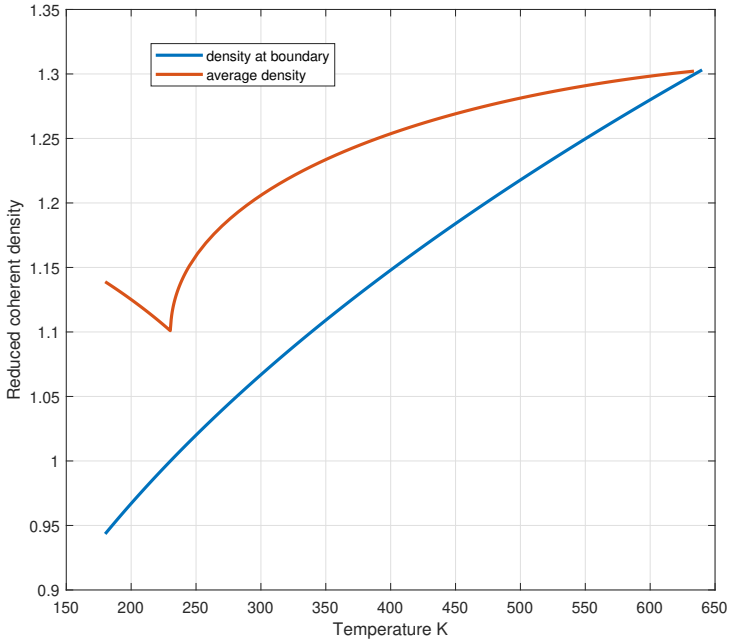

Figure 7. Reduced coherent density at the boundary and in the bulk of the coherent phase as a function of temperature.

The average density within the CD can be calculated by integrating over the volume:

$$< \hat{\rho}_c(T) >= \frac{\int_0^{\phi_{vol}(T)} \hat{\rho}_c(\phi'_{vol})\, d\phi'_{vol}}{\phi_{vol}(T)} \tag{25}$$

and the result is shown in Figure 7 (orange curve).

Finally, the molar coherent fraction, shown in Figure 6, is determined by:

$$\phi_{mol}(T) = \frac{< \hat{\rho}_c(T) > \phi_{vol}(T)\rho_0}{< \hat{\rho}_c(T) > \phi_{vol}(T)\rho_0 + (1 - \phi_{vol}(T))\rho_n(T)} \tag{26}$$

where $\rho_n(T)$ is the density of the normal (incoherent) phase.

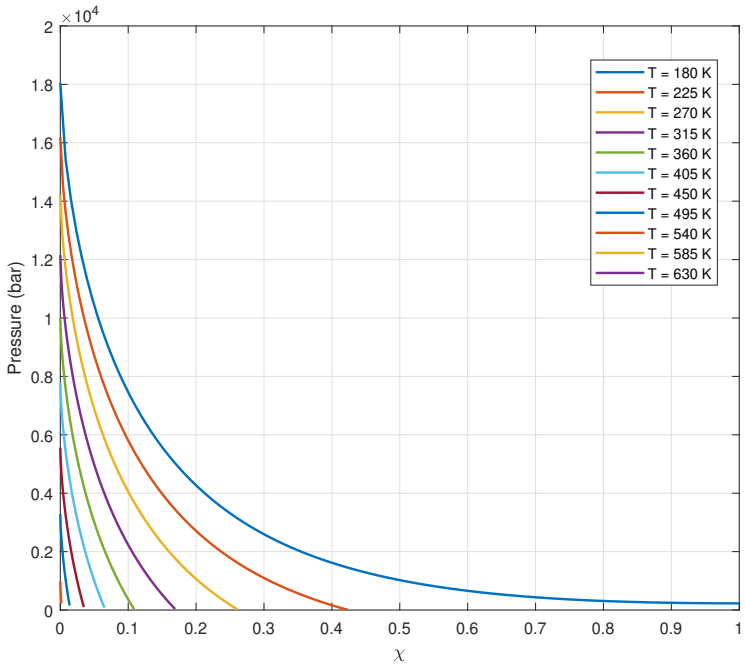

Figure 8. Reduced density profile within the coherent domain showing increased density towards the center due to compression effects. The absence of an intersection between the density profile and the x-axis indicates that, at ≈228 K, the system exhibits complete coherence $\phi_{mol}(228K) = 1$.

3. Part II

3.1. Thermodynamic Properties

In this section, we present the thermodynamic properties of liquid water derived from the theoretical framework developed in this work. Although not all the calculated quantities accurately reproduce the experimental data, the main focus lies in the theory's ability to capture the general trends and qualitative behaviors of these properties as a function of thermodynamic parameters such as pressure and temperature. The simplicity and effectiveness of the present theory in capturing the overall trends of liquid water's thermodynamic behavior, despite some quantitative discrepancies primarily arising from the limitations of the vdW model, underscore its utility in providing fundamental insights into the complex nature of water. By bridging quantum coherence with classical thermodynamics, the framework offers a robust foundation for understanding water's anomalies, paving the way for future refinements and applications.

The following calculations illustrate the predictive capacity of our theory and its relevance in understanding the general thermodynamic landscape of water under varying conditions.

3.2. Parameter Optimization

The theory depends on a number of parameters whose values are not known with high precision. Given this uncertainty, a parameter optimization procedure was carried out by minimizing the mean squared error between certain thermodynamic quantities predicted by the theory and the corresponding experimental values over a range of temperatures.

The objective function used in the optimization is defined as

$$E_{\text{tot}} = E(\text{density}) + E(\text{compressibility}) + E(\text{dielectric constant}), \tag{27}$$

where $E(q)$ denotes the mean normalized squared error associated with a given thermodynamic quantity q, and is defined by

$$E(q) = \frac{1}{N}\sum_{i=1}^{N}\left[\frac{q(T_i)}{q_{\exp}(T_i)} - 1\right]^2, \tag{28}$$

with N representing the number of experimental data points available for quantity q, and T_i the corresponding temperatures.

The parameters selected for optimization are indicated in Table 2, together with their optimized values.

The objective function was minimized using a MATLAB (2020a) routine based on the `FMINCON` optimization function.

Table 2. Parameter values and their respective units.

Parameter	Value	Units
electric dipole for vapor	1.84	D
mass of water molecule	$1.7280 \cdot 10^{10}$	eV
T_{crit}	0.0554	eV
P_{crit} (fit parameter)	$2.17 \cdot 10^{6}$	eV^4
reference coherent density ρ_0 (fit parameter)	$2.12 \cdot 10^{8}$	eV^3
coherent energy gap δ_{0c} (fit parameter)	0.29	eV
$\delta_{c,dd}$ (fit parameter)	0.2	eV
$\delta_{c,LJ}$ (fit parameter)	0.066	eV

3.3. Density and Thermal Expansion Coefficient

The density anomaly is probably the most puzzling behavior of water. It is at the base of life in the oceans and contributes to determine the climate on Earth. Unlike most other liquids, water exhibits a maximum density at 4° C under ambient pressure and expands when cooled below this temperature.

In our theory, at temperature T the molecular volume of liquid water is the weighted average of the molecular volumes of the coherent and incoherent phases, the weight being the volumetric coherent fraction $\phi_{vol}(T)$

$$v_{H_2O}(T) = \phi_{vol}(T)v_c(T) + (1 - \phi_{vol}(T))v_n(T). \tag{29}$$

The density is therefore

$$\rho_{H_2O} = \frac{\rho_c\rho_n}{\phi_{vol}(\rho_n - \rho_c) + \rho_c}. \tag{30}$$

where $\rho_{c,n} = \frac{1}{v_{c,n}}$. The computed density along the liquid-vapor curve of coexistence is shown in Figure 9. In Figure 10 is shown the computed isobaric thermal expansion coefficient.

The anomaly arises from the fact that, when temperature decreases, the increasing density of the incoherent phase is balanced by the decrease of its fraction, leading to the existence of a maximum

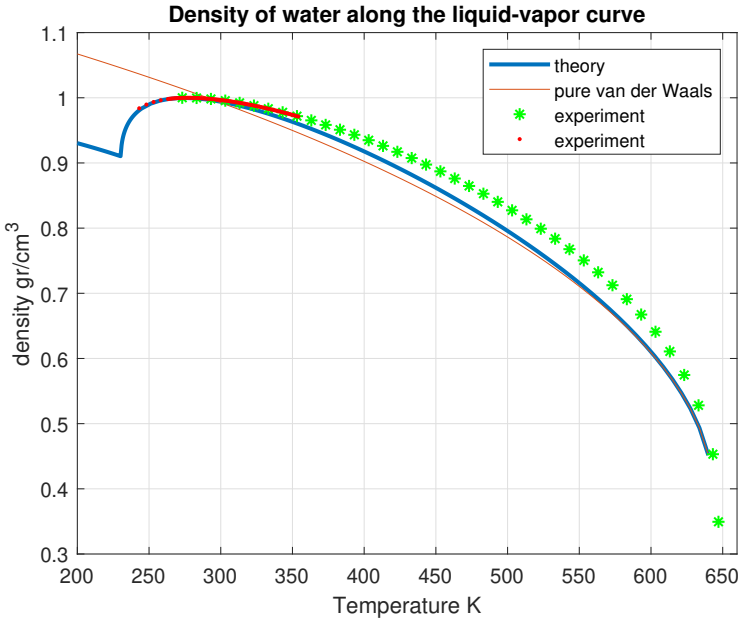

Figure 9. Computed density of liquid water as a function of temperature along the liquid–vapor coexistence curve, compared with the experimental data [25].

of the density which happens to be at 4 °C at atmospheric pressure.

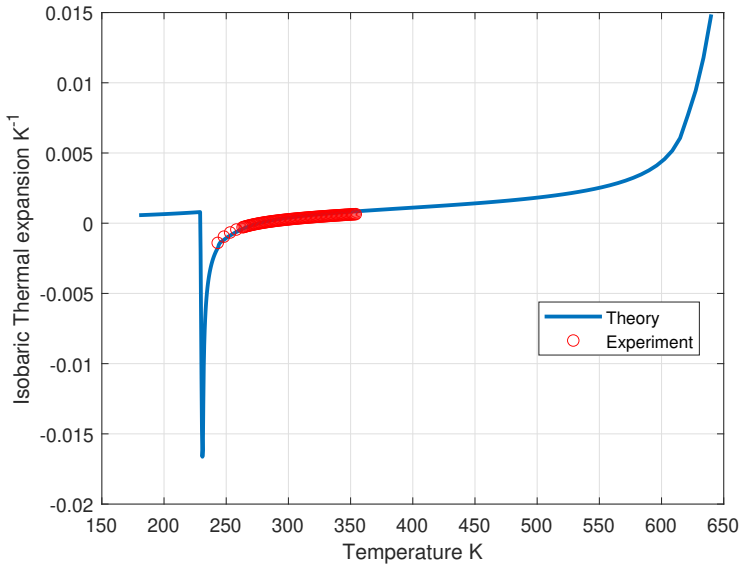

Figure 10. Computed isobaric thermal expansion of liquid water as a function of temperature along the liquid-vapor coexistence curve compared with experimental data [25].

3.4. Isobaric Heat Capacity

An intriguing and yet to be elucidated characteristic of liquid water pertains to its isobaric heat capacity per particle (IHCP), which exhibits a notable minimum at a temperature of 309 K under standard atmospheric pressure and a sharp decrease in the range 228–235 K [25,26]. In our theoretical framework, the contribution to the IHCP arises from the standard incoherent component and the vibrational degrees of freedom of water molecules, supplemented by the additional contribution of the coherent molecules transitioning out of the zero-temperature state and migrating towards the incoherent phase. This latter contribution becomes particularly significant at low temperatures, where the derivative of ϕ_{mol} increases sharply, and is absent in existing models of liquid water's IHCP to date.

The enthalpy resulting from the contribution of the two phases can be written as

$$h(T) = \phi_{mol}(T)h_c(T) + (1 - \phi_{mol}(T))h_n(T), \tag{31}$$

where

$$h_{c,n}(T) = f_{c,n}(T) - Ts_{c,n}, \tag{32}$$

where $s_{c,n}$ are the entropies of the coherent and incoherent phases respectively. s_c corresponds to the entropy of the vibrational configurations only, being the positional degrees of freedom frozen at zero temperature by their coherent nature, so that we can write $s_c = s_{c,vib}$.

The IHCP is given by

$$c_p = \left(\frac{\partial h(T)}{\partial T}\right)_P. \tag{33}$$

It is instructive to examine in detail the various terms contributing to the IHCP by expanding Equation (31). The IHCP may be expressed as the sum of the following components:

$$\begin{aligned} c_{p,c} &= \left(\frac{\partial \phi_{mol}}{\partial T}\right)_P (h_c - h_n) \\ c_{p,vib,c} &= \phi_{mol}\left(\frac{\partial h_c}{\partial T}\right)_P \\ c_{p,n} &= (1 - \phi_{mol})\left(\frac{\partial h_n}{\partial T}\right)_P. \end{aligned} \tag{34}$$

It is interesting to note that the term $c_{p,c}$ is analogous to a "latent heat" of transformation from the coherent to the incoherent phase, modulated by the rate of change of the coherent phase with temperature and accounts for the sharp increase of the IHCP at low temperature.

The relationship between the chemical potential and the enthalpy per particle is given by $\mu_{c,n} = h_{c,n} - Ts_{c,n}$, where $s_{c,n}$ denotes the entropy of the coherent and incoherent phases. Given the equality of the chemical potentials for the two phases, the following relations hold

$$c_{p,c} = T\left(\frac{\partial \phi_{mol}}{\partial T}\right)_P (-s_{vdW} + s_{c,vib} - s_{n,vib}) \tag{35a}$$

$$c_{p,vib,c} = \phi_{mol} \sum_i g_{c,i} \frac{\omega_{c,i}^2}{4T^2 \sinh^2 \frac{\omega_{c,i}}{2T}} \tag{35b}$$

$$c_{p,n} = (1 - \phi_{mol})\left(\left(\frac{\partial h_{vdW}}{\partial T}\right)_P + \sum_i g_{n,i} \frac{\omega_{n,i}^2}{4T^2 \sinh^2 \frac{\omega_{n,i}}{2T}}\right). \tag{35c}$$

Here $c_{p,c}$ represents the contribution from particles transitioning from the coherent to the incoherent phase, with the difference primarily arising from entropy variation.

The coherent and incoherent vibrational terms of the entropy are given by the standard expression for the harmonic oscillator

$$s_{c,n,vib} = \sum_i g_{c,n,i} \left\{ \frac{\omega_{c,n,i}}{T} \frac{1}{e^{\frac{\omega_{c,n,i}}{T}} - 1} - \log\left(1 - e^{-\frac{\omega_{c,n,i}}{T}}\right) \right\}, \tag{36}$$

where $g_{c,n,i}$ and $\omega_{c,n,i}$ are taken from Table 1.

Equation (35a) depends on the absolute entropy of the incoherent phase. However, the entropy s_{vdW} of a vdW fluid is inherently defined only up to an additive constant s_0, since its low-temperature behavior becomes intrinsically quantum and deviates from the classical expression, which exhibits a logarithmic divergence as temperature approaches zero. To address this, we introduce a constant term into the vdW entropy expression, which will later be calibrated against experimental data.

Accordingly, Equation (35a) is reformulated as

$$c_{p,c} = -\left(\frac{\partial \phi_{mol}}{\partial T}\right)_P (h_{\mathrm{vdW}} - \mu_{\mathrm{vdW}} + T(s_{c,\mathrm{vib}} - s_{n,\mathrm{vib}} - s_0)), \tag{37}$$

where the entropy is expressed in terms of the known quantities μ_{vdW} and h_{vdW} using the relation $\mu = h + Ts$. The constant s_0 has been introduced to account for the aforementioned uncertainty in the absolute value of the vdW entropy.

The expression in (35b) originates from the thermal capacity of the quantum oscillators with strength $g_{c,i}$ and oscillation frequency $\omega_{c,i}$, as described in Table 1.

Finally, the formula in (35c) represents the contribution of the vdW and vibrational components within the incoherent phase. The explicit expression for the temperature derivative of the vdW enthalpy at constant pressure can be obtained through straightforward algebraic manipulation, leading to

$$\left(\frac{\partial h_{\mathrm{vdW}}}{\partial T}\right)_P = \frac{3}{2} - \frac{4\,\frac{T}{T_{\mathrm{crit}}}}{\hat{\rho}^3 - 6\,\hat{\rho}^2 + 9\,\hat{\rho} - 4\,\frac{T}{T_{\mathrm{crit}}}}. \tag{38}$$

The calculation of $c_p(T)$ is shown in Figure 11 where we have chosen $s_0 = 6$ and where are detailed also the contributions of the three terms of Equations (35).

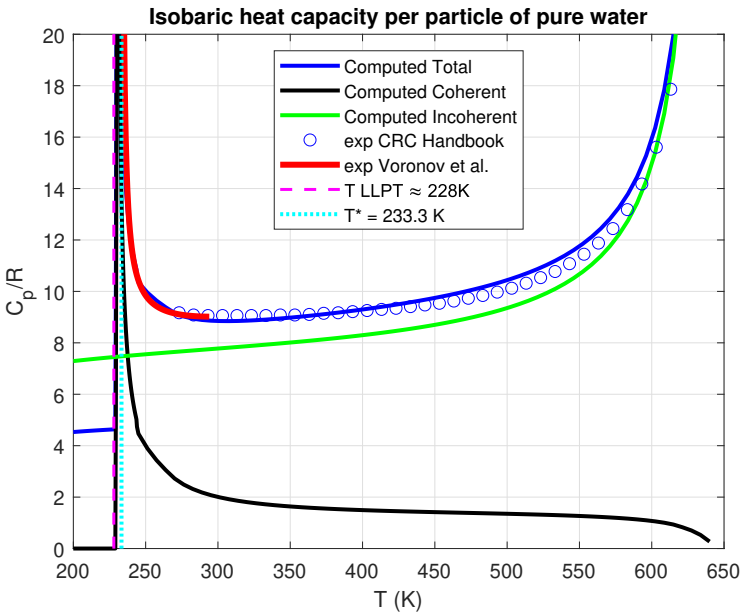

Figure 11. Isobaric heat capacity per particle of liquid water as a function of temperature at atmospheric pressure compared with experimental data [26].

The computed values deviate from experimental measurements by less than 10% on average. The calculation accurately reproduces the existence of the minimum—a distinctive hallmark of liquid water's IHCP and, more importantly, the sharp increase of c_p in the thermal range 228–235 K. To this day, this phenomenon lacks a fully satisfactory explanation in the literature. However, we believe that our theory captures its essential nature by merely evaluating the temperature derivative of enthalpy.

3.5. Isothermal Compressibility

The isothermal compressibility of liquid water has historically been one of the puzzling properties of water [8]. The anomaly is characterized by a minimum in compressibility at 319 K, which still lacks a structural explanation.

In our approach, this anomaly finds a natural explanation, attributed to the differing behavior of the two phases. The isothermal compressibility $\kappa_T(T)$ is defined as

$$\kappa_T(T) = -\frac{1}{v}\left(\frac{\partial v}{\partial P}\right)_T, \tag{39}$$

where v is the volume per molecule, P is the pressure, and T is the temperature.

This expression can be rewritten by considering the contribution of the two phases:

$$\kappa_T(T) = -\frac{1}{v}\left(\frac{\partial[\phi_{vol}(T)(v_c - v_n) + v_n]}{\partial P}\right)_T, \tag{40}$$

where ϕ_{vol} represents the volumetric fraction of the coherent phase, v_c and v_n are the volumes per particle of the coherent and incoherent phases, respectively.

The derivatives with respect to pressure of ϕ_{vol}, v_c, and v_n can all be evaluated numerically, given that their expressions are known. Specifically, ϕ_{vol} depends on pressure via Equation (24), while v_c and v_n are determined by the equations of state (12) and (18), respectively.

By performing the numerical differentiation at constant temperature and substituting the results into Equation (40), we obtain the outcome depicted in Figure 12, where a minimum is clearly visible and a sharp increase at lower temperatures with a peak at ≈228 K.

The computed values of the compressibility do not accurately reproduce the experimental data for κ_T, since the van der Waals model is highly inaccurate in calculating κ_T for the incoherent phase. Nonetheless, the inclusion of the coherent contribution captures both the presence of a minimum and the divergence of κ_T at the temperature of the liquid–liquid critical point (LLCP).

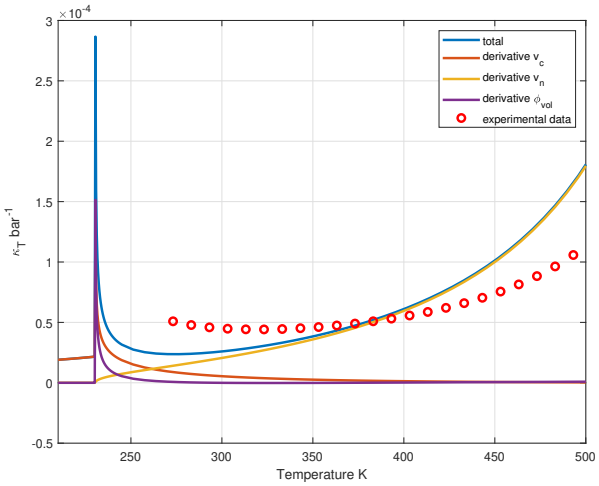

Figure 12. Isothermal compressibility of liquid water as a function of temperature along the coexistence curve. A minimum is observed, consistent with the experimental observations. The calculation is affected by a certain degree of approximation, as it relies on the van derWaals equation of state, which provides only a crude description of the non-coherent phase.

3.6. Static Dielectric Constant

Liquid water exhibits an unusually large static dielectric constant, which is difficult to reproduce within conventional models without invoking strong approximations. Our quantum electrodynamical (QED) framework, however, provides a natural and quantitatively accurate description of this property as a function of temperature.

3.6.1. Coherent Contribution to the Dielectric Response

The coherent electronic state in the absence of an electric field is described as a quantum superposition of the molecular ground state $|GS\rangle$ and an excited $|5d\rangle$ state:

$$|\text{coh}, 0\rangle = \cos\alpha\,|GS\rangle + \sin\alpha\,|5d\rangle, \tag{41}$$

with α quantifying the mixing amplitude and the state normalized to unity.

When an external electric field $\vec{E}$ is applied, the interaction Hamiltonian in the dipole approximation reads

$$H_{\text{int}} = -e\int_{V_{CD}} d^3\vec{x}\,(\vec{x}\cdot\vec{E}), \tag{42}$$

where V_{CD} is the volume of a coherence domain and e the elementary charge. In Appendix A, a detailed first-order calculation of the interaction term is carried out, and a descriptive discussion is provided below.

The induced macroscopic polarization $\vec{P}$ is computed as the expectation value of the position operator over the field-perturbed coherent state $|\text{coh}, E\rangle$:

$$\vec{P} = \frac{eN_c}{V_{CD}}\int_{V_{CD}} d^3\vec{x}\,\langle\text{coh}, E|\vec{x}|\text{coh}, E\rangle, \tag{43}$$

where N_c is the number of coherent electrons.

Expanding to second order in the field, the polarization separates into three contributions (see Appendix A for a detailed calculation):

$$\vec{P} = \vec{P}_1 + \vec{P}_2 + \vec{P}_3 + O(e^4), \tag{44}$$

with

$$\vec{P}_1 \propto \cos^2\alpha \quad \text{(ground-state deformation)}, \tag{45a}$$
$$\vec{P}_2 \propto \cos\alpha\sin\alpha \quad \text{(cross-term)}, \tag{45b}$$
$$\vec{P}_3 \propto \sin^2\alpha \quad \text{(dominant contribution from the excited state)}. \tag{45c}$$

The term $\vec{P}_1$ yields a negligible polarization density $\vec{P}_1 = \hat{\rho}_c\eta_{c1}\vec{E}$ with $\eta_{c1} \approx 0.095$, due to the large energy gap between the ground state and higher excitations. The mixed term $\vec{P}_2 = \hat{\rho}_c\eta_{c2}\vec{E}$ is also negligible with $\eta_{c2} \approx 0.12$ (see appendix A). In contrast, $\vec{P}_3$ is substantial: the excited $|5d\rangle$ state (at $\omega_{5d} = 12.06$ eV) lies close to a dense manifold of unperturbed molecular levels, resulting in small energy denominators in the second-order expansion formula (see Appendix A) that amplify the response.

Since the oscillator strengths $f_{n,5d}$ are not directly known, we model the excited spectrum near 12 eV as that of a harmonic oscillator with level spacing $\Delta\omega = 0.21$ eV, based on the energy levels of the intermediate states close to 12.06 eV reported in Table A1.

Using standard harmonic oscillator matrix elements and the relation $x = (a + a^\dagger)/\sqrt{2\Delta\omega\, m_e}$, the sum over intermediate states simplifies to (see Appendix A)

$$\vec{P}_3 = \frac{2e^2N_c\sin^2\alpha}{V_{CD}\,\Delta\omega^2\,m_e}\,\vec{E} = \hat{\rho}_c\eta_{c3}\,\vec{E}, \tag{46}$$

where $\hat{\rho}_c = N_c/(V_{CD}\rho_0)$ is the normalized density of the coherent phase and $\rho_0 = 2.12 \times 10^8\text{eV}^3$ is the reference density.

Substituting numerical values ($e^2 = 0.0917$, $\sin^2\alpha = 0.10$, $m_e = 5.11 \times 10^5$ eV, $\Delta\omega = 0.21$ eV) yields

$$\eta_c = \eta_{c1} + \eta_{c2} + \eta_{c3} \simeq 167.$$

By defining the coherent susceptibility as $\chi_c = \hat{\rho}_c \eta_c$, we find that at room temperature $\chi_c \simeq 200$. This value should be compared with the experimentally measured value of $\sim$156 at room temperature, where a two-phase dielectric model was employed to fit the experimental data [27].

3.6.2. Total Dielectric Constant

The static dielectric constant of liquid water is then obtained by combining the coherent and incoherent contributions according to their molar fractions:

$$\varepsilon(T) = 1 + \phi_{\mathrm{mol}}(T)\,\chi_c + \big(1 - \phi_{\mathrm{mol}}(T)\big)\,\chi_n(T), \tag{47}$$

where the incoherent susceptibility follows the Debye–Langevin expression [28]:

$$\chi_n(T) = \frac{\mu^2 \rho_n(T)}{3T} \quad (\approx 12 \quad \text{at } 300\ \mathrm{K}). \tag{48}$$

As shown in Figure 13, the resulting temperature dependence reproduces the experimental trend and predicts a kink in $\varepsilon(T)$ at the same critical temperature where thermodynamic response functions (e.g., isothermal compressibility, heat capacity) have a singular behavior.

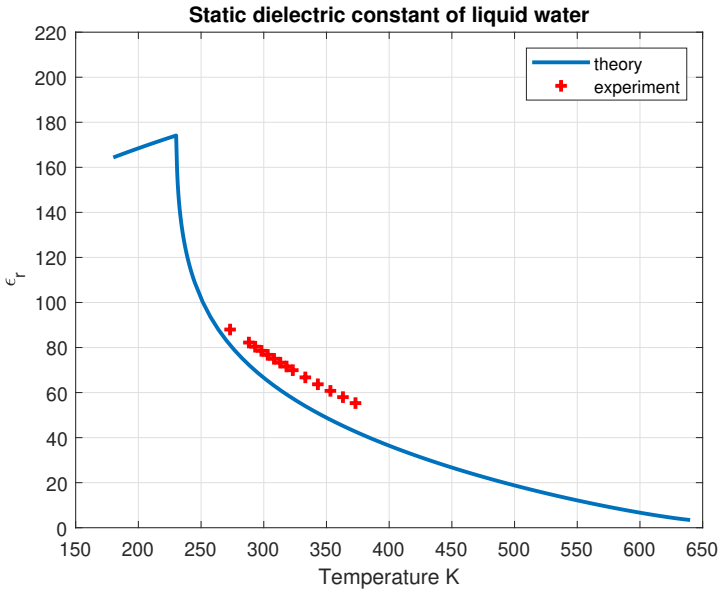

Figure 13. Static dielectric constant of liquid water along the liquid–vapor coexistence curve. The solid line shows the prediction of the two-phase QED picture. The result is subject to a certain level of approximation, primarily due to the use of a harmonic oscillator model to estimate the response of the excited electronic manifold.

It is worthwhile observing that this result leads to an important physical insight: the application of a strong static electric field shifts the thermodynamic equilibrium between the coherent and incoherent phases of liquid water in favor of the coherent one. Within our quantum electrodynamical framework, at ambient temperature the coherent phase exhibits a markedly higher static dielectric permittivity ($\chi_c \approx 200$, Equation (46)) compared to the incoherent phase ($\chi_n \approx 12$ at ambient temperature, Equation (48)). Because the coherent phase is far more polarizable, its expansion under an external field lowers the system's free energy, thereby increasing the fraction of the coherent phase. This field-induced enhancement of coherence offers a natural explanation for the emergence of ice-like structural features, and dramatically reduced molecular mobility—phenomena

recently observed in ab initio molecular dynamics simulations of water under intense electric fields of 0.10–0.15 V Å^{-1} [29].

This mechanism may also be highly relevant in biological contexts. Structured "vicinal" water is routinely observed adjacent to hydrophilic surfaces such as cellular membranes, exhibiting reduced diffusivity and spectroscopic signatures consistent with an increased coherent fraction. Notably, endogenous electric fields near biological membranes can reach intensities of $\sim 10^5$ V/m (i.e., 0.1 V Å^{-1})—precisely the threshold at which simulations report the onset of "electrofreezing," characterized by the development of low-density amorphous (LDA)-like radial distribution functions and a 12.5-fold reduction in diffusivity [29]. Thus, our framework suggests that the ubiquitous presence of ordered interfacial water in living systems may arise not only from surface chemistry but also from field-driven thermodynamic stabilization of the coherent phase.

4. Discussion and Conclusions

To achieve a comprehensive understanding of the origin of water's behavior, particularly the properties that make it the most vital liquid for the existence of life on Earth, we have developed a theory grounded rigorously in the first principles of quantum electrodynamics (QED). This theoretical framework enables us to address a fundamental question that has intrigued physicists in recent years: is water a homogeneous or an inhomogeneous fluid?

It is instructive to compare our quantum electrodynamical (QED) two-phase picture with the widely discussed LDL/HDL (low- and high-density liquid) scenario, which interprets water's anomalies in terms of fluctuating local structural motifs supported by scattering, spectroscopy, and molecular simulations. While both frameworks invoke a duality in liquid water, their physical foundations differ substantially. In the LDL/HDL view, the distinction arises from the topology and dynamics of the hydrogen-bond network, governed by empirical or semi-empirical intermolecular potentials. In contrast, the QED approach attributes phase coexistence to spontaneous symmetry breaking of the quantum electromagnetic field, yielding a thermodynamically stable coherent phase (low-density-like, highly polarizable) and an incoherent phase (high-density-like, weakly polarizable).

A compelling model proposed by Nilsson and Pettersson [8] describes liquid water as a mixture of two interconverting structural motifs: a tetrahedral, low-density liquid (LDL) and a distorted, high-density liquid (HDL). This two-state picture is supported by various experimental and computational techniques. However, within this framework, the physical mechanism by which these local, fluctuating structures could give rise to distinct, metastable macroscopic phases remains unclear.

Our theory challenges the conventional view that hydrogen bonding serves as the fundamental explanation for the behavior of liquid water. This traditional perspective relies heavily on the empirical adjustment of parameters such as bond lifetime and strength, rather than deriving them from first principles. Consequently, such models are not genuine theories but phenomenological approximations that offer only partial and descriptive insights into the nature of liquid water.

Within our QED-based framework, the hydrogen bond is not a primary interaction but an emergent phenomenon. It arises from the combination of two effects: (i) the deformation of the electronic charge distribution in water molecules that are part of a Coherence Domain (CD), and (ii) a collective, density-dependent attractive force generated by the coherent interaction with the self-trapped electromagnetic field. As shown in Equation (2), this deformation induces a directional angular dependence in the electronic charge density, naturally accounting for the tetrahedral coordination of water molecules observed in neutron and X-ray scattering experiments [4]. Furthermore, the disappearance

of hydrogen bonding at elevated temperatures is consistent with our theoretical predictions: as temperature rises, the proportion of coherent molecules diminishes, leading to the weakening and eventual disappearance of hydrogen bonding.

On the mesoscopic scale, CDs exhibit a striking organizational duality. While adopting a hexagonal close-packed (HCP) arrangement (see Figures 1 and 2), the system simultaneously preserves fluidity through lubricated sliding mediated by the incoherent phase. This coexistence of structural order and dynamic disorder resolves the long-standing paradox of water's anomalous viscoelastic properties, which combine long-range electromagnetic coherence with short-range molecular mobility.

So far, no direct experimental evidence has confirmed the existence of Coherence Domains (CDs). Nevertheless, a wide range of independent experimental observations consistently support the idea that liquid water exhibits a morphic structure with a characteristic length scale on the order of $\sim 100\,\text{nm}$.

The experimental results summarized in Table 3 reveal systematic deviations in the physical properties of water under nanoscale confinement. The anomalous increase in viscosity was first observed in carbon nanotubes by Secchi et al. [30]; within our theoretical framework, this effect can be interpreted as the absence of the lubricating incoherent phase that typically enables the CDs to easily slide along the capillary boundaries. A reduction of the dielectric constant in nanoconfined water was directly measured using scanning probe techniques by Fumagalli et al. [31]. Molecular diffusion anomalies were investigated by Coridan et al. [32] through X-ray photon correlation spectroscopy using surface-sensitive methods. Both sets of results can be interpreted as the suppression of CDs when the confining size falls below the wavelength of the resonant coherent electromagnetic field, thereby preventing their formation.

Table 3. Reported deviations of water's physical properties observed at length scales below 100 nm. These anomalies—affecting viscosity, dielectric constant, diffusion, and other key properties—indicate the presence of nanoscale structural organization in water.

Property	Deviation	Scale (nm)	Ref.
Viscosity	↑ up to 100×	<100	[30]
Dielectric constant	↓ down to <30	<100	[31]
Diffusion	↓ 2–10×	<100	[32]
Heat capacity	↑ increased	< 200	[33,34]
Density	± variable	<100	[35]
Ionic conductivity	↓ reduced	<100	[36,37]
Freezing point	↓ −10 to −30 K	<50	[38]
Local pH	altered	<100	[39]

Additional experimental signatures, not yet fully analyzed within our theoretical framework, include anomalous heat capacity and interfacial vibrational effects reported by Tombari et al. [33] and Angell et al. [34]; density variations in hydrophilic and hydrophobic nanopores measured via neutron scattering by Zhang et al. [35]; and ionic conductivity anomalies reported in single-layer boron nitride nanotubes by Siria et al. [36], as well as in sub-nanometer carbon pores by Tunuguntla et al. [37].

Further phenomena include the depression of the freezing point, studied theoretically and experimentally by Alabarse [38], and local pH alterations due to charge-induced ion partitioning explored by Liu et al. [39]. Taken together, these studies establish a consistent transition in the macroscopic properties of water when confined below the $\sim 100\,\text{nm}$ scale, thereby providing strong evidence for the existence of structural organizations at this characteristic length scale.

It is important to note that CDs, as predicted by the QED theory, are not static, stable structures but dynamic, fluctuating entities. This inherent nature makes direct microscopic visualization of individual domains extremely challenging, and evidence for their existence relies on indirect observations consistent with a two-fluid interpretation of water's properties.

For completeness, we note that several experimental studies have reported results that do not provide evidence for stable, well-defined nanometric structures in bulk liquid water. For instance, high-resolution X-ray diffraction and spectroscopic analyses suggest that water at ambient conditions exhibits a fluctuating hydrogen-bond network consistent with a largely homogeneous liquid rather than the coexistence of distinct, static nanoscale domains [5,40]. Similarly, ultrafast X-ray probing of supercooled water droplets indicates a continuous increase in structural order upon cooling, without clear signatures of stable phase-separated clusters at the nanometric scale [41]. These observations, however, remain compatible with our theoretical framework since, in the two-phase picture, coherence domains (CDs) exist in a statistical sense and are not rigid, isolated entities. Instead, there is a continuous dynamical exchange of molecules between the coherent and incoherent fractions, which naturally reconciles the absence of sharply separated nanostructures in certain experimental probes with the presence of underlying coherence phenomena.

In summary, the significance of this work lies in the introduction of three foundational advances:

1. It elucidates the physical mechanisms underlying the formation and stability of the distinct liquid phases. The coherent low-density liquid (LDL) phase arises via spontaneous symmetry breaking of the electromagnetic field, resulting in macroscopic quantum domains with an average size of $\sim$50 nm characterized by an energy gap $\delta_c \simeq 0.3\,\mathrm{eV}$ and a spatial distribution described by the spherical Bessel function j_0. The HDL phase, described as a polar van der Waals fluid, fills the interstices between domains. Our solutions quantitatively determine the relative abundances of these phases over a range of temperatures, reinterpreting the so-called liquid–liquid phase transition (LLPT) not as a true critical phenomenon, but rather as the temperature threshold—upon cooling—at which the incoherent phase (HDL) vanishes.
2. The theory offers a first-principles explanation for several of water's most perplexing anomalies. The well-known density maximum at 277 K emerges from the competition between the volumetric expansion of LDL domains and the densification of the HDL phase. The observed minimum in the isobaric heat capacity near 309 K reflects a balance between the stabilization of the coherent phase and thermal excitation. Most notably, the theory accounts for the sharp divergence in thermodynamic behavior near 228 K as a consequence of the complete disappearance of the HDL fraction.
3. The theory resolves the longstanding quantum–classical duality exhibited by water. Below approximately 320 K, the system demonstrates macroscopic quantum coherence through extended networks of coherence domains, while simultaneously retaining classical fluidity through the intervening HDL phase. As temperature increases, the coherent fraction diminishes, leading to the gradual loss of quantum coherence and explaining the crossover to purely classical behavior near the critical point.

Future work to refine the theoretical framework presented here should address several key areas. While the foundational structure of the theory originates from first-principles QED arguments, a detailed parametrization is currently required to describe the short-range properties of water molecules. This concerns, for example, the Lennard-Jones potentials of both the coherent and incoherent phases (which necessarily differ due to the distinct electronic structures of the two phases), as well as the dipole–dipole interaction. Moreover, the critical pressure of the van der Waals (vdW) model deviates from the experimental

value, since it depends on the vdW parameters a and b, which are specific to the incoherent phase. These short-range aspects, while sufficient for the present conceptual framework, could be systematically refined in future work.

Although the vdW model provides a simple and insightful starting point, it remains a mean-field approximation. The primary objective of this study has been to establish a foundational theoretical perspective on the nature of liquid water rather than to reproduce all thermodynamic properties in exact detail. Once this conceptual basis is solidified, further refinements can be introduced to capture the full complexity of water phenomenology.

A more rigorous treatment of the incoherent phase would involve modeling it as a manifestation of quantum fluctuations in the matter field, represented by quasi-particle excitations. This approach aligns with the framework of quantum fluids, in which excitations correspond to fluctuations around the mean-field background. Finally, significant uncertainty remains regarding the internal molecular dynamics, particularly the energetics of vibrational modes. These degrees of freedom play a critical role in determining the thermodynamic properties of water and must be accurately characterized to improve the predictive power and quantitative accuracy of the theory.

Our results demonstrate that the anomalous properties of liquid water arise from its dual character: a quantum-coherent system coexisting with quantum thermal fluctuations. This paradigm not only resolves several long-standing thermodynamic anomalies, but also opens new avenues for research, particularly in the study of biological water interfaces and the development of quantum-inspired materials. The dynamic interplay between coherence and decoherence in water may prove to be a fundamental principle underlying its unique role in both natural processes and emerging technologies.

Author Contributions: Conceptualization, A.D.N. and L.G.; Software, L.G.; Formal analysis, A.D.N. and L.G.; Writing—original draft, A.D.N. and L.G.; Writing—review and editing, A.D.N. and L.G. All authors contributed equally and All authors have read and agreed to the published version of the manuscript.

Funding: This research received no external funding.

Data Availability Statement: The data presented in this study are theoretical values generated by numerical codes developed by the authors. All relevant results are included in the article; therefore, no additional data are available.

Conflicts of Interest: The author Luca Gamberale is employed by the company Quantumatter Inc., the remaining author declares no conflicts of interest.

Appendix A. Detailed Derivation of the Coherent Contribution to the Static Dielectric Constant

In this appendix, we provide a derivation of the coherent contribution to the static dielectric constant of liquid water within the quantum electrodynamical (QED) framework. The calculation proceeds from the interaction of the coherent electronic state with an external static electric field $\vec{E}$, through perturbation theory, to the evaluation of the macroscopic polarization.

Appendix A.1. Coherent State and Interaction Hamiltonian

The electronic state inside a Coherence Domain (CD) of volume V_{CD} is described as a quantum superposition of the molecular ground state $|GS\rangle$ and an excited $|5d\rangle$ state:

$$|\mathrm{coh}, 0\rangle = \cos\alpha\,|GS\rangle + \sin\alpha\,|5d\rangle, \tag{A1}$$

where α is the mixing angle and the state is normalized:

$$\langle \text{coh}, 0 | \text{coh}, 0 \rangle = 1. \tag{A2}$$

The interaction with a static external electric field $\vec{E}$ is treated in the dipole approximation. The interaction Hamiltonian reads:

$$H_{\text{int}} = -e \int_{V_{CD}} d^3\vec{x}\, (\vec{x} \cdot \vec{E}), \tag{A3}$$

where e is the elementary charge.

Appendix A.2. Perturbed Coherent State

To first order in time-independent perturbation theory, the field-perturbed coherent state is:

$$|\text{coh}, E\rangle = |\text{coh}, 0\rangle + \sum_{n \neq \text{coh}} \frac{\langle n | H_{\text{int}} | \text{coh}, 0 \rangle}{\omega_{\text{coh}} - \omega_n} |n\rangle, \tag{A4}$$

where $|n\rangle$ are excited molecular states with energies ω_n, and $\omega_{\text{coh}} = -0.29$ eV is the energy of the coherent state. The excited $|5d\rangle$ state has energy $\omega_{5d} = 12.06$ eV.

Evaluating the matrix element using the dipole form of H_{int} and expressing the position operator via oscillator strengths, we obtain:

$$\begin{aligned} |\text{coh}, E\rangle &= |\text{coh}, 0\rangle - e \sum_{n \neq \text{coh}} \frac{\left\langle n \middle| \int_{V_{CD}} d^3\vec{x} \left(\vec{x} \cdot \vec{E}\right) \middle| \text{coh}, 0 \right\rangle}{\omega_{\text{coh}} - \omega_n} |n\rangle \\ &= |\text{coh}, 0\rangle - eE \sum_{n \neq \text{coh}} \frac{1}{\sqrt{2m_e}(\omega_{\text{coh}} - \omega_n)} \\ &\quad \times \left(\cos\alpha \sqrt{\frac{f_{n0}}{\omega_n - \omega_0}} + \sin\alpha \sqrt{\frac{f_{n,5d}}{\omega_n - \omega_{5\text{d}}}} \right) |n\rangle. \end{aligned} \tag{A5}$$

where $f_{ij} = 2m_e(\omega_i - \omega_j)|\langle i|\hat{x}|j\rangle|^2$ denotes the oscillator strength between states i and j, ω_0 is the ground-state energy (set to zero), and m_e is the electron mass.

Appendix A.3. Macroscopic Polarization

The macroscopic polarization is defined as the expectation value of the dipole density:

$$\vec{P} = \frac{eN_c}{V_{CD}} \int_{V_{CD}} d^3\vec{x}\, \langle \text{coh}, E | \vec{x} | \text{coh}, E \rangle, \tag{A6}$$

with N_c the number of coherent electrons per domain.

Expanding to second order in e, the polarization splits into three contributions:

$$\vec{P} = \vec{P}_1 + \vec{P}_2 + \vec{P}_3 + O(e^4), \tag{A7}$$

where

$$\vec{P}_1 = -\frac{2e^2 N_c \cos^2\alpha}{2m_e V_{CD}} \sum_{n \neq 0, n_{5d}} \frac{f_{n0}}{(\omega_{\text{coh}} - \omega_n)(\omega_n - \omega_0)} \vec{E}, \tag{A8a}$$

$$\vec{P}_2 = -\frac{2e^2 N_c \cos\alpha \sin\alpha}{2m_e V_{CD}} \sum_{n \neq 0, n_{5d}} \frac{1}{(\omega_{\text{coh}} - \omega_n)} \sqrt{\frac{f_{n0} f_{n,5d}}{(\omega_n - \omega_0)(\omega_n - \omega_{5d})}} \vec{E}, \tag{A8b}$$

$$\vec{P}_3 = -\frac{2e^2 N_c \sin^2\alpha}{2m_e V_{CD}} \sum_{n \neq 0, n_{5d}} \frac{f_{n,5d}}{(\omega_{\text{coh}} - \omega_n)(\omega_n - \omega_{5d})} \vec{E}. \tag{A8c}$$

- $\vec{P}_1$ represents the polarizability of the ground state. Its contribution is small due to the large energy gap between the ground state and higher-lying excitations. All the quantities in Equation (A8a) are known so that $\vec{P}_1$ is easily evaluated to be $\vec{P}_1 = \hat{\rho}_c \eta_{c1}$ with $\eta_{c1} = 0.095$.
- $\vec{P}_2$ is a cross-term coupling the ground and excited components. This term remains relatively small because it involves the product of oscillator strengths centered at widely separated energies, and it is further suppressed by a large energy difference in the denominator.
- $\vec{P}_3$ provides the dominant contribution, as the energy denominator $\omega_n - \omega_{5d}$ becomes small for states in the vicinity of the $|5d\rangle$ resonance, leading to a significant enhancement of the response.

Table A1. Experimental oscillator strengths f_{0n} for water vapor. Data above 11 eV are used to estimate the level spacing $\Delta\omega$ in the harmonic oscillator model for the $|5d\rangle$ manifold.

eV	f_{0n}
7.400	0.0500
9.700	0.0732
10.000	0.0052
10.170	0.0140
10.350	0.0107
10.560	0.0092
10.770	0.0069
11.000	0.0218
11.120	0.0223
11.385	0.0098
11.523	0.0086
11.772	0.0178
12.074	0.0101
12.243	0.0053
12.453	0.0025

Appendix A.4. Evaluation of $\vec{P}_2$ and $\vec{P}_3$ via Harmonic Oscillator Approximation

Since the oscillator strengths $f_{n,5d}$ are not known a priori, we approximate the excited spectrum near $\omega_{5d} = 12.06$ eV as that of a quantum harmonic oscillator with level spacing $\Delta\omega$ by making use of the formula $f_{ij} = 2m_e(i-j)\Delta\omega|\langle i|\hat{x}|j\rangle|^2$. From the experimental energy levels listed in Table A1, we restrict attention to levels above 11 eV and find an average spacing of $\Delta\omega = 0.21$ eV and $n_{5d} \sim 54$.

For a harmonic oscillator, the position operator is

$$x = \frac{a + a^\dagger}{\sqrt{2m_e\Delta\omega}}, \tag{A9}$$

and the matrix elements satisfy

$$\left\langle n \middle| a + a^\dagger \middle| 5d \right\rangle = (n+1)\delta_{n,n_{5d}-1} + n\delta_{n,n_{5d}+1}, \tag{A10}$$

where $\delta_{nn'}$ is the Kroneker symbol.

Using this, the sum in $\vec{P}_2$ becomes:

$$\vec{P}_2 = \frac{2e^2 N_c \sin\alpha\cos\alpha}{2m_e V_{CD}} \sum_{n\neq n_{5d}} \frac{|\langle n|x|5d\rangle|}{\omega_n - \omega_{\text{coh}}} \sqrt{\frac{2m_e\Delta\omega f_{0n}(n-n_{5d})}{(\omega_n-\omega_0)(\omega_n-\omega_{5d})}}\,\vec{E}. \tag{A11}$$

Approximating $\omega_n - \omega_{\text{coh}} \approx \overline{\omega} \approx n_{5d}\Delta\omega$ and evaluating the sum over n, we obtain:

$$\vec{P}_2 \simeq \frac{2e^2 N_c \sin\alpha\cos\alpha}{2m_e V_{CD}} \sum_{n\neq n_{5d}} \frac{|\langle n|a+a^\dagger|5d\rangle|}{\omega_n - \omega_{\text{coh}}} \sqrt{\frac{f_{0n}}{n_{5d}\Delta\omega^2}}\,\vec{E} \tag{A12}$$

and using Equation (A10)

$$\vec{P}_2 \simeq \frac{2e^2 N_c \sin\alpha\cos\alpha}{2m_e V_{CD}} \sum_{n\neq n_{5d}} \frac{|\langle n|a+a^\dagger|5d\rangle|}{n_{5d}\Delta\omega^2} \sqrt{\frac{f_{0n}}{n_{5d}}}\,\vec{E} \tag{A13}$$

so that

$$\vec{P}_2 \simeq \frac{e^2 N_c \sin\alpha\cos\alpha}{m_e V_{CD}\Delta\omega^2 n_{5d}^{3/2}} \left(\sqrt{f_{0,n_{5d}-1}} + \sqrt{f_{0,n_{5d}+1}}\right)\vec{E} \tag{A14}$$

Introducing the normalized coherent number density $\hat{\rho}_c = N_c/(V_{CD}\rho_0)$, with $\rho_0 = 2.12 \times 10^8$ eV^3, we write:

$$\vec{P}_2 = \hat{\rho}_c\,\eta_{c2}\,\vec{E}, \tag{A15}$$

where

$$\eta_{c2} = \frac{e^2 \sin\alpha\cos\alpha}{m_e\Delta\omega^2 n_{5d}^{3/2}} \left(\sqrt{f_{0,n_{5d}-1}} + \sqrt{f_{0,n_{5d}+1}}\right), \tag{A16}$$

Likewise, the sum in $\vec{P}_3$ becomes:

$$\vec{P}_3 = \frac{2e^2 N_c \sin^2\alpha}{V_{CD}} \sum_{n\neq n_{5d}} \frac{|\langle n|x|5d\rangle|^2}{\omega_n - \omega_{\text{coh}}}\vec{E}. \tag{A17}$$

Approximating $\omega_n - \omega_{\text{coh}} \approx \overline{\omega} \approx n_{5d}\Delta\omega$ and evaluating the sum over n, we obtain:

$$\sum_{n\neq 5d} |\langle n|a+a^\dagger|5d\rangle|^2 = 2n_{5d} + 1 \approx 2n_{5d}, \tag{A18}$$

so that

$$\vec{P}_3 = \frac{2e^2 N_c \sin^2\alpha}{V_{CD}\,\Delta\omega^2\,m_e}\,\vec{E}. \tag{A19}$$

Introducing the normalized coherent number density $\hat{\rho}_c = N_c/(V_{CD}\rho_0)$, with $\rho_0 = 2.12 \times 10^8$ eV^3, we write:

$$\vec{P}_3 = \hat{\rho}_c\,\eta_{c3}\,\vec{E}, \tag{A20}$$

where η_{c3} is given by:

$$\eta_{c3} = \frac{2e^2\rho_0 \sin^2\alpha}{\Delta\omega^2 m_e}. \tag{A21}$$

References

1. Röntgen, W.C. Ueber die Constitution des flüssigen Wassers. *Ann. Phys.* **1892**, *281*, 91–97. [CrossRef]
2. Poole, P.H.; Sciortino, F.; Essmann, U.; Stanley, H.E. Phase behaviour of metastable water. *Nature* **1992**, *360*, 324–328. [CrossRef]
3. Mishima, O.; Stanley, H.E. The relationship between liquid, supercooled and glassy water. *Nature* **1998**, *396*, 329–335. [CrossRef]
4. Wernet, P.; Nordlund, D.; Bergmann, U.; Cavalleri, M.; Odelius, M.; Ogasawara, H.; Naslund, L.A.; Hirsch, T.K.; Ojamae, L.; Glatzel, P.; et al. The structure of the first coordination shell in liquid water. *Science* **2004**, *304*, 995–999. [CrossRef]
5. Huang, C.; Wikfeldt, K.T.; Tokushima, T.; Nordlund, D.; Harada, Y.; Bergmann, U.; Niebuhr, M.; Weiss, T.M.; Horikawa, Y.; Leetmaa, M.; et al. The inhomogeneous structure of water at ambient conditions. *Proc. Natl. Acad. Sci. USA* **2009**, *106*, 15214–15218. [CrossRef]
6. Taschin, A.; Bartolini, P.; Eramo, R.; Righini, R.; Torre, R. Evidence of two distinct local structures of water from ambient to supercooled conditions. *Nat. Commun.* **2013**, *4*, 2401. [CrossRef]

7. Gallo, P.; Amann-Winkel, K.; Angell, C.A.; Anisimov, M.A.; Caupin, F.; Chakravarty, C.; Lascaris, E.; Loerting, T.; Panagiotopoulos, A.Z.; Russo, J.; et al. Water: A Tale of Two Liquids. *Chem. Rev.* **2016**, *116*, 7463–7500. [CrossRef]
8. Nilsson, A.; Pettersson, L. The structural origin of anomalous properties of liquid water. *Nat. Commun.* **2015**, *6*, 8998. [CrossRef]
9. Stillinger, F.H.; Rahman, A. Improved Simulation of Liquid Water by Molecular Dynamics. *J. Chem. Phys.* **1974**, *60*, 1545–1557. [CrossRef]
10. Paesani, F. Getting the Right Answers for the Right Reasons: Toward Predictive Molecular Simulations of Water with Many-Body Potential Energy Functions. *Acc. Chem. Res.* **2016**, *49*, 1844–1851. [CrossRef]
11. Sciortino, F.; Zhai, Y.; Bore, S.L.; Paesani, F. Constraints on the Location of the Liquid–Liquid Critical Point in Water. *Nat. Phys.* **2025**, *21*, 480–485. [CrossRef]
12. Yasutomi, M. Thermodynamic mechanism of the density and compressibility anomalies of water in the range $-30 < T\ (°C) < 100$. *Sci. Rep.* **2022**, *12*, 1219. [CrossRef] [PubMed]
13. Del Giudice, E.; Preparata, G.; Vitiello, G. Water as a free electric dipole laser. *Phys. Rev. Lett.* **1988**, *61*, 1085–1088. [CrossRef] [PubMed]
14. Preparata, G. *QED Coherence in Matter*; World Scientific: Singapore, 1995.
15. Bono, I.; Del Giudice, E.; Gamberale, L.; Henry, M. Emergence of the Coherent Structure of Liquid Water. *Water* **2012**, *4*, 510–532. [CrossRef]
16. Arani, R.; Bono, I.; del Giudice, E.; Preparata, G. QED coherence and the thermodynamics of water. *Int. J. Mod. Phys. B* **1995**, *9*, 1813–1841. [CrossRef]
17. Ninno, A.D.; Giudice, E.D.; Gamberale, L.; Castellano, A.C. The Structure of Liquid Water Emerging from the Vibrational Spectroscopy: Interpretation with QED Theory. *Water* **2014**, *6*, 13–25.
18. Del Giudice, E.; Vitiello, G. The role of the electromagnetic field in the formation of domains in the process of symmetry breaking phase transitions. *Phys. Rev. A* **2006**, *74*, 022105. [CrossRef]
19. De Ninno, A.; De Francesco, M. Water molecules ordering in strong electrolytes solutions. *Chem. Phys. Lett.* **2018**, *705*, 7–11. [CrossRef]
20. Majolino, D.; Mallamace, F.; Migliardo, P.; Aliotta, F.; Micali, N.; Vasi, C. Spectral evidence of connected structures in liquid water: Effective Raman density of vibrational states. *Phys. Rev. E* **1993**, *47*, 2454–2459. [CrossRef]
21. Buzzacchi, M.; Del Giudice, E.; Preparata, G. Coherence of the Glassy State. *Int. J. Mod. Phys. B* **2002**, *16*, 3771–3786. [CrossRef]
22. Del Giudice, E.; Galimberti, A.; Gamberale, L.; Preparata, G. Electrodynamical Coherence in Water: A Possible Origin of the Tetrahedral Coordination. *Mod. Phys. Lett. B* **1995**, *09*, 953–961. [CrossRef]
23. Johnston, D.C. *Advances in Thermodynamics of the van der Waals Fluid*; Morgan & Claypool Publishers: San Rafael, CA, USA, 2014; pp. 2053–2571. [CrossRef]
24. Gregory, J.K.; Clary, D.C.; Liu, X.; Brown, M.; Saykally, R.J. The water dipole moment in water clusters. *Science* **1997**, *275*, 814–817. [CrossRef]
25. Haynes, W.M., Ed. *CRC Handbook of Chemistry and Physics*, 97th ed.; CRC Press: Boca Raton, FL, USA, 2016.
26. Voronov, V.P.; Podnek, V.E.; Anisimov, M.A. High-resolution adiabatic calorimetry of supercooled water. *J. Phys. Conf. Ser.* **2019**, *1385*, 012008. [CrossRef]
27. De Ninno, A.; Nikollari, E.; Missori, M.; Frezza, F. Dielectric permittivity of aqueous solutions of electrolytes probed by THz time-domain and FTIR spectroscopy. *Phys. Lett. A* **2020**, *384*, 126865. [CrossRef]
28. Jackson, J.D. *Classical Electrodynamics*, 3rd ed.; Chapters 4 and 8 for Detailed Discussion on Dielectric Polarization and the Langevin Function; John Wiley & Sons: New York, NY, USA, 1998.
29. Cassone, G.; Martelli, F. Electrofreezing of liquid water at ambient conditions. *Nat. Commun.* **2024**, *15*, 1856. [CrossRef] [PubMed]
30. Secchi, E.; Marbach, S.; Niguès, A.; Stein, D.; Siria, A.; Bocquet, L. Massive radius-dependent flow slippage in carbon nanotubes. *Nature* **2016**, *537*, 210–213. [CrossRef] [PubMed]
31. Fumagalli, L.; Esfandyarpour, A.; Gabini, R.; Kolasinski, R.; Stein, D.; Albrecht, T.; Geim, A.; Bocquet, L.; Grosjean, G. Anomalously low electronic dielectric constant in confined water. *Science* **2018**, *362*, 159–162.
32. Coridan, R.H.; Schmidt, N.W.; Lai, G.H.; Abbamonte, P.; Wong, G.C.L. Dynamics of confined water reconstructed from inelastic x-ray scattering measurements of bulk response functions. *Phys. Rev. E* **2012**, *85*, 031501. [CrossRef]
33. Tombari, E.; Salvetti, G.; Ferrari, C.; Johari, G.P. Heat capacity of water in nanopores. *J. Chem. Phys.* **2005**, *123*, 214706. [CrossRef]
34. Angell, C.A.; Shuppert, J.; Tucker, J.C. Anomalous properties of supercooled water. Heat capacity, expansivity, and proton magnetic resonance chemical shift from 0 to −38%. *J. Phys. Chem.* **1973**, *77*, 3092–3099. [CrossRef]
35. Zhang, Y.; Faraone, A.; Kamitakahara, W.A.; Liu, K.H.; Mou, C.Y.; Leão, J.B.; Chang, S.; Chen, S.H. Density hysteresis of heavy water confined in a nanoporous silica matrix. *Proc. Natl. Acad. Sci. USA* **2011**, *108*, 12206–12211. [CrossRef]
36. Siria, A.; Poncharal, P.; Biance, A.L.; Fulcrand, R.; Blase, X.; Purcell, S.T.; Bocquet, L. Giant osmotic energy conversion measured in a single transmembrane boron nitride nanotube. *Nature* **2013**, *494*, 455–458. [CrossRef]

37. Tunuguntla, R.H.; Henley, R.Y.; Yao, Y.C.; Pham, T.A.; Wanunu, M.; Noy, A. Enhanced water permeability and tunable ion selectivity in subnanometer carbon nanotube porins. *Science* **2017**, *357*, 792–796. [CrossRef]
38. Alabarse, F.G.; Haines, J.; Cambon, O.; Levelut, C.; Bourgogne, D.; Haidoux, A.; Granier, D.; Coasne, B. Freezing of Water Confined at the Nanoscale. *Phys. Rev. Lett.* **2012**, *109*, 035701. [CrossRef] [PubMed]
39. Liu, H.S.; Zhang, X.M.; Liang, G.H.; Zheng, S.; Li, J.F. Investigation of water structure and proton transfer within confined graphene by ab initio molecule dynamics and multiscale data analysis. *Chin. J. Struct. Chem.* **2025**, *44*, 100596. [CrossRef]
40. Tokushima, T.; Harada, Y.; Takahashi, O.; Senba, Y.; Ohashi, H.; Pettersson, L.; Nilsson, A.; Shin, S. High resolution X-ray emission spectroscopy of liquid water: The observation of two structural motifs. *Chem. Phys. Lett.* **2008**, *460*, 387–400. [CrossRef]
41. Perakis, F.; Amann-Winkel, K.; Lehmkühler, F.; Sprung, M.; Mariedahl, D.; Sellberg, J.A.; Pathak, H.; Späh, A.; Cavalca, F.; Schlesinger, D.; et al. Diffusive dynamics during the high-to-low density transition in amorphous ice. *Proc. Natl. Acad. Sci. USA* **2017**, *114*, 8193–8198. [CrossRef]